

Haptic Control of a Mobile Robot: A User Study

Sangyoon Lee[†] Gaurav S. Sukhatme[‡] Gerard Joung Hyun Kim[†] Chan-Mo Park[†]

[†]*Virtual Reality Laboratory
Dept. of Computer Science & Engineering
Pohang University of Science and Technology (POSTECH)
Pohang, Kyungbuk, 790-784 South Korea
sylee|gkim|parkcm@postech.ac.kr*

[‡]*Robotic Embedded Systems Laboratory
Dept. of Computer Science
University of Southern California
Los Angeles, CA 90089-0781 USA
gaurav@usc.edu*

Abstract

We address the problem of teleoperating a mobile robot using shared autonomy: an on-board controller performs obstacle avoidance while the operator uses the manipulandum of a haptic probe to designate the desired speed and rate of turn. Sensors on the robot are used to measure obstacle range information. We describe a strategy to convert such range information into forces, which are reflected to the operator's hand, via the haptic probe. This haptic information provides feedback to the operator in addition to imagery from a front-facing camera mounted on the mobile robot. Extensive experiments with a user population show that the added haptic feedback significantly improves operator performance in several ways (reduced collisions, increased minimum distance between the robot and obstacles) without a significant increase in navigation time.

1 Introduction

Teleoperation is often employed in controlling mobile robots navigating in unknown and unstructured environments. This is largely because teleoperation makes use of the sophisticated cognitive capabilities of the human operator [1, 2].

However, for navigation in dynamic environments or at high-speeds, it is often desirable to provide a sensor-based collision avoidance scheme on-board the robot to guarantee safe navigation. Without such a collision avoidance scheme, it would be difficult for the (remote) operator to prevent the robot from colliding with obstacles. This is primarily due to (1) limited information from the robot's sensors, such as images within a restricted viewing angle without depth information, which is insufficient for the users' full perception of the environment in which the robot moves [3], and (2) significant delay in the communication channel between the operator and the robot.

The implementation of a collision avoidance scheme

on-board the robot can cause conflict between the user's actions and the movement of the robot. For example, consider a situation where the operator directly controls the movement of a mobile robot with a joystick and the robot is supposed to move forward when the user pushes the stick forward. Imagine that the robot is also programmed with a simple collision avoidance algorithm to avoid obstacles. If an obstacle exists in front of the robot, the robot may stop or turn in order to avoid collision, although the operator is clearly commanding it to move ahead. In this example, the conflict may be not a problem if the user can easily see the obstacles. If however, the obstacles are invisible due to a restricted viewing angle, the user might be confused since the robot does not move nor act according to the teleoperation commands.

We hypothesize that the conflict can be naturally resolved by exploiting haptic information, that is, by providing the operator with force feedback. In this paper, we measure the utility of force feedback in a mobile robot teleoperation system for safe navigation and to resolve conflicting goals. Our experiments (conducted using a virtual environment) measure the extent to which haptic information helps an operator in safely navigating a mobile robot. The experiments clearly show that the added haptic feedback significantly improves operator performance in several ways (reduced collisions, increased minimum distance between the robot and obstacles) without a significant increase in navigation time.

This paper is structured as follows. In Section 2, we describe related work in the area of haptic information for navigation. In Sections 3 and 4, we describe the use of the haptic device for commanding the robot and the force rendering algorithm, respectively. Section 5 deals with the implementation of a control system providing force feedback. In Sections 6 and 7, we describe our experiment and results. We conclude with a summary and a discussion of fu-

ture work.

2 Related Work

Force-feedback has long been used for precise remote control in teleoperation of manipulators [4, 5]. Recently, with the spread of commercial haptic devices such as the PHANTOM [6], the CyberGrasp [7], and various force-feedback joysticks [8], haptic information is being used in many areas of virtual reality, robotics, training and entertainment. Primarily haptic feedback is used as a supplementary cue to help the user understand the virtual environment [9, 10, 11, 12, 13].

In [14], the authors used artificial force fields for navigation in virtual environments. Their work neither provides force feedback to users, nor was it applied to guiding mobile robots. However, they showed that force fields help make navigation comfortable. In [15], the authors proposed an algorithm for haptic navigation within volumetric datasets. Although their aim was to understand the structure of volumetric datasets (rather than effective navigation), their force-rendering method was similar to ours for rendering the environmental force, in that distance fields were used.

For mobile robot navigation, an event-based direct control with force feedback was proposed in [16, 11]. This approach reflected the difference between the actual velocity and the desired velocity of the mobile robot to the operator as force feedback. The conflict between the operator’s command and the actual movement of the robot was resolved to some degree. However, it was difficult to perform precise navigation in a cluttered environment with their method since the turn rate was not considered for force rendering and collision avoidance was automatically performed compelling the robot to stop at the distance of $0.5m$ from obstacles.

A full range of advanced interfaces for vehicle control has been investigated by [17]. In particular, HapticDriver [3] had the same aims as ours. They informally showed that HapticDriver improved obstacle detection and collision avoidance in vehicle teleoperation. However, they also did not consider collision avoidance while turning.

3 Car-Driving Metaphor

We use a car-driving metaphor for direct control of a mobile robot. This metaphor can be applied to most mobile robots that support turning in place. A logical point (x, z) (obtained by projecting the 3D haptic probe location to a xz -plane) is mapped to motion parameters such as speed and turning rate (Figure 1) as follows:

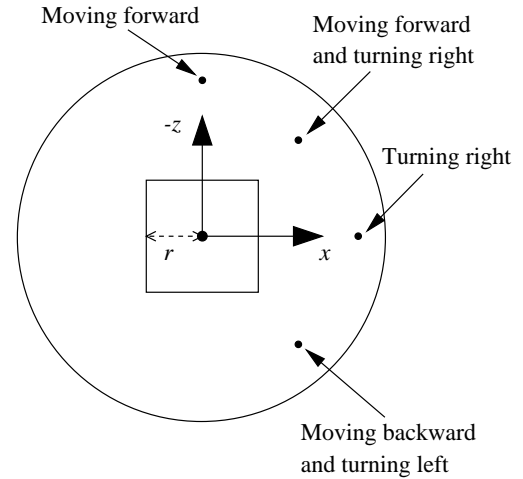


Figure 1: Car-driving metaphor: mapping a logical point (x, z) to motion parameters (speed rate s , turning rate θ).

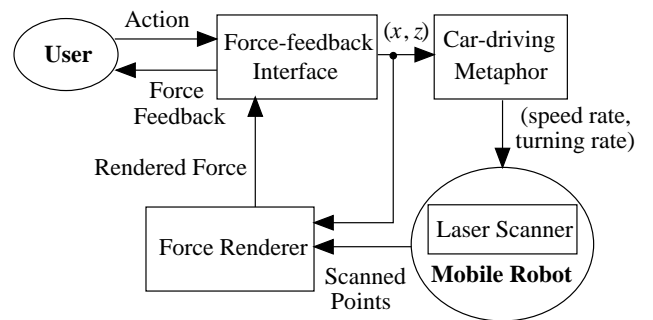


Figure 2: Force feedback from the user’s action.

$$\text{speed } s = k_1 \cdot h(-z, r) \quad (1)$$

$$\text{turning rate } \theta = \begin{cases} k_2 \cdot h(x, r), & \text{if } z \leq r \\ k_2 \cdot h(-x, r), & \text{if } z > r \end{cases} \quad (2)$$

$$\text{where } h(a, r) = \begin{cases} a - r & \text{if } a > r \\ a + r & \text{if } a < -r \\ 0 & \text{if } |a| \leq r \end{cases}$$

Note that $s = 0$ when the logical point is in the area where $|z| \leq r$, and the turning rate $\theta = 0$ when the logical point is in the area where $|x| \leq r$. This dead-zone prevents movement of the robot due to small unintended user actions and tremors. Although we use a linear function, other monotonic functions such as quadratic or cubic functions can be used. Note that the speed has positive values where $z < -r$ since we use a coordinate system in which the value of z is negative in front. k_1 and k_2 are proportionality constants.

4 Force Rendering

Force rendering is the process of computing the force that the operator in contact with the haptic device feels. In direct control, the user's action (i.e. designating the logical position of the haptic probe) is used to determine the speed and turning rate of the robot.

When the user determines the logical position, the force that the user should feel at that position is computed from the position information of the obstacles surrounding the robot. A laser scanner attached to the robot obtains the position information of the obstacles represented as a list of distance values between the robot and the obstacles. Figure 2 shows the process to feed back the force from the user's action.

We consider two kinds of forces: an "environmental" force and a "collision-preventing" force. Let the environmental force and the collision-preventing force be represented by $(F_{e,x}, F_{e,z})$ and $(F_{c,x}, F_{c,z})$ respectively. The final rendered force (F_x, F_z) is given by:

$$(F_x, F_z) = (\max\{F_{e,x}, F_{c,x}\}, \max\{F_{e,z}, F_{c,z}\}) \quad (3)$$

The max function returns the value that has the largest absolute value.

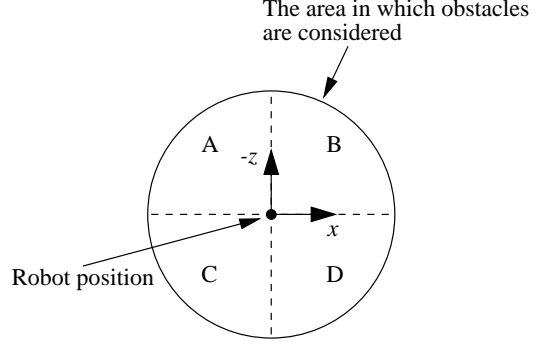
4.1 Environmental Force

The environmental force prevents the robot from moving and turning towards obstacles by giving the user the distance information between the robot and the obstacles in a form of force.

This force is similar to the traditional potential force field used for path planning of mobile robots [18]. However, the environmental force is different from the potential force in some aspects. First, there is no attraction to a goal since we assume that the goal position is unknown. Secondly, only obstacles in the "relevant" area (according to the logical position of the interface) are considered, i.e. the obstacles that are for, or in the direction opposite to the movement of the robot are not relevant. Figure 3 shows areas that are considered according to the position of the interface and intended direction of the robot. Finally, and most importantly, instead of the average or the sum of the forces due to obstacles, the maximum force over all obstacles is used since it is difficult to make the user recognize the differences of the distances between the robot and the obstacles if the average or the sum is used.

When the logical position of the interface is represented by (x, z) , the environmental force $\mathbf{F}_e = (F_{e,x}, F_{e,z})$ is given by:

$$F_{e,x} = \begin{cases} k_3 f_{-x}(D)x & \text{if } x \geq 0 \\ -k_3 f_{+x}(D)x & \text{if } x < 0 \end{cases} \quad (4)$$



Considered Areas	Condition
A and B	$z < 0$ (moving forward)
C and D	$z > 0$ (moving backward)
A and C	$x < 0$ (turning left)
B and D	$x > 0$ (turning right)

Figure 3: Obstacles considered according to the movement of the robot.

$$F_{e,z} = \begin{cases} k_4 f_{-z}(D)x & \text{if } z \geq 0 \\ -k_4 f_{+z}(D)x & \text{if } z < 0 \end{cases} \quad (5)$$

where

$$f_{-x}(D) = \max_{i=1}^n [\phi_{-x}(d_i) \frac{d_i - r_{\max}}{r_{\max}} \cos \theta_i]$$

$$f_{+x}(D) = \max_{i=1}^n [\phi_{+x}(d_i) \frac{d_i - r_{\max}}{r_{\max}} \cos \theta_i]$$

$$f_{-z}(D) = \max_{i=1}^n [\phi_{-z}(d_i) \frac{d_i - r_{\max}}{r_{\max}} \sin \theta_i]$$

$$f_{+z}(D) = \max_{i=1}^n [\phi_{+z}(d_i) \frac{d_i - r_{\max}}{r_{\max}} \sin \theta_i]$$

$$\phi_{-x}(d_i) = \begin{cases} 1 & \text{if } d_i < r_{\max} \text{ and } \cos \theta_i > 0 \\ 0 & \text{otherwise} \end{cases}$$

$$\phi_{+x}(d_i) = \begin{cases} 1 & \text{if } d_i < r_{\max} \text{ and } \cos \theta_i < 0 \\ 0 & \text{otherwise} \end{cases}$$

$$\phi_{-z}(d_i) = \begin{cases} 1 & \text{if } d_i < r_{\max} \text{ and } \sin \theta_i > 0 \\ 0 & \text{otherwise} \end{cases}$$

$$\phi_{+z}(d_i) = \begin{cases} 1 & \text{if } d_i < r_{\max} \text{ and } \sin \theta_i < 0 \\ 0 & \text{otherwise} \end{cases}$$

$$D = \{d_1, d_2, \dots, d_n\}$$

The function f_{+z} represents the maximum value of the z components for all the forces due to the obstacles in the front area of the robot (Figure 4), and is used when the robot is moving forward. This value is more than 0, so that the robot is prevented from moving closer to obstacles when the user intends the

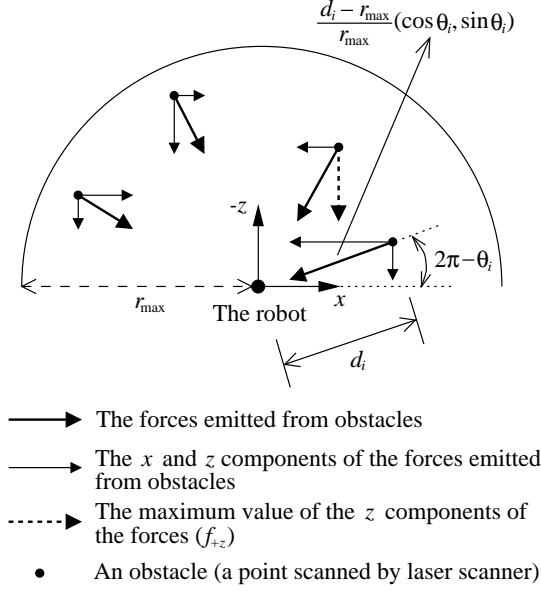


Figure 4: An example of f_{+z} (The local coordinate system of the robot is used.)

robot to move forward. The functions f_{-z} , f_{+x} and f_{-x} are defined similarly, and are applied when the robot is moving backward, turning left, and turning right, respectively.

The force due to an obstacle is inversely proportional to the distance d_i between the robot and the obstacle, and does not affect the robot when the distance is equal to or more than r_{\max} . By changing r_{\max} , the user can adjust the range within which the force emitted from the obstacle affects the robot. Note that we consider each scanned point obtained from the laser scanner as an obstacle.

k_3 and k_4 are the constants to adjust the magnitude of the force. If these constants have large values, it is hard to control the robot since the rendered force is too large although the robot is far away from obstacles. On the other hand, if the constants are too small, the operator does not feel any force. We use $k_3 = k_4 = 0.1$, which are determined empirically.

Although the environmental force prevents the robot from moving and turning towards obstacles to some degree, it does not guarantee that the robot will not collide with any obstacles. This is because the robot is modeled as a point, while, in actuality, the robot can have any shape and an obstacle is modeled as a polygon whose vertices are the scanned points obtained by the laser scanner. The force just slows the robot down where obstacles are near the robot. To guarantee collision-free navigation, we introduce the collision-preventing force.

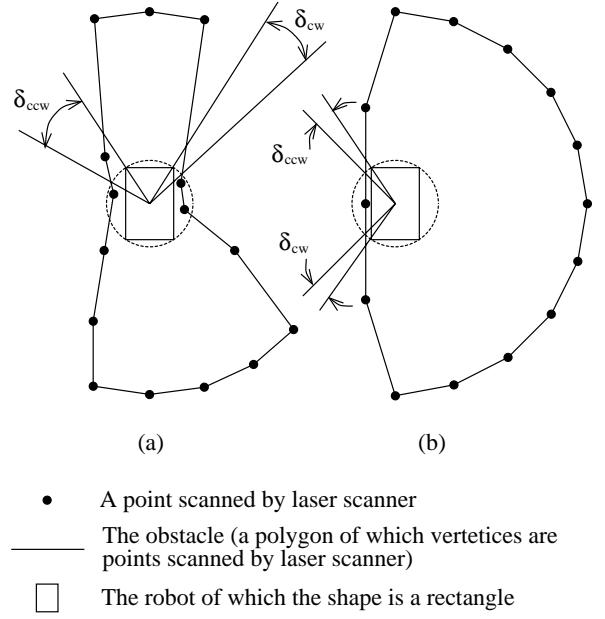


Figure 5: Two examples of the left and right possible-turning angles (δ_{ccw} and δ_{cw}).

4.2 Collision-Preventing Force

The collision-preventing force is computed from possible-turning angles and the distances between the robot and the obstacles in the front and rear direction of the robot. The possible-turning angles are the maximum angles by which the robot can turn without any collision. These angles have two types: the left (or counter-clockwise) angle (δ_{ccw}) and the right (or clockwise) angle (δ_{cw}) since the robot can turn both left and right. Figure 5 shows two examples of the possible-turning angles for a rectangular-shaped robot.

The distances between the robot and the obstacle in the front and rear direction of the robot are the maximum distances (d_{front} and d_{rear}) by which the robot can move forward and backward without any collision. Figure 6 shows an example of these distances.

When the logical position of the interface is represented by (x, z) , the collision-preventing force $\mathbf{F}_c = (F_{c,x}, F_{c,z})$ is given by:

$$F_{c,x} = \begin{cases} k_5 \frac{\delta_{avg} - \delta_{ccw}}{\delta_{avg}} x & \text{if } x \geq 0 \text{ and } \delta_{avg} - \delta_{cw} > 0 \\ k_5 \frac{\delta_{avg} - \delta_{cw}}{\delta_{avg}} x & \text{if } x < 0 \text{ and } \delta_{avg} - \delta_{ccw} > 0 \end{cases} \quad (6)$$

$$F_{c,z} = \begin{cases} k_6 \frac{d_{front} - d_{max}}{d_{max}} z & \text{if } d_{front} < d_{max} \text{ and } z \leq 0 \\ -k_6 \frac{d_{rear} - d_{max}}{d_{max}} z & \text{if } d_{rear} < d_{max} \text{ and } z > 0 \\ 0 & \text{otherwise} \end{cases} \quad (7)$$

where

$$\delta_{avg} = \frac{\delta_{ccw} + \delta_{cw}}{2}$$

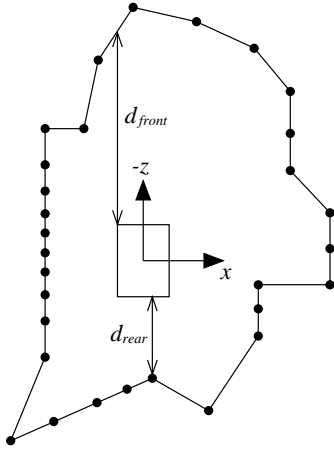


Figure 6: An example of d_{front} and d_{rear} (The local coordinate system of the robot is used.)

The absolute value of the z component, $F_{c,z}$, of the collision-preventing force is inversely proportional to d_{front} when the robot is moving forward and d_{rear} when the robot is moving backward. By sending this component of the force to the user when the robot is moving towards an obstacle, a collision can be prevented. The user can control the speed and turnrate of the robot without any disturbance when the robot is at a certain distance equal to or more than d_{max} from obstacles.

The x component $F_{c,x}$ of the force is to prevent the robot from colliding with obstacles when the user intends the robot to turn left or right. Unlike $F_{c,z}$, $F_{c,x}$ is computed by using a relative difference of the left and right possible-turning angles. Consider the case shown in Figure 5(b) in which both the left and right possible-turning angles are very small since the side of the robot is close to a wall. If absolute differences as in Equation (7) were used, it would be difficult for the user to make the robot turn in any direction because a large force would be sent to the user in order to prevent the robot from colliding with the wall by turning. This means that the user could control only the speed of the robot, allowing the robot to only follow the wall and making it difficult for the user to change the distance between the robot and the wall. By using the relative difference, however, the user can change the heading of the robot to some degree, alleviating this problem. We use $k_5 = k_6 = 0.3$, which are determined empirically.

5 Implementation

We implemented a direct control system for the Activmedia Pioneer 2-DX mobile robots equipped with the SICK LMS-200 laser scanner and the Sony EVID-30 camera. The laser scanner provides a scan

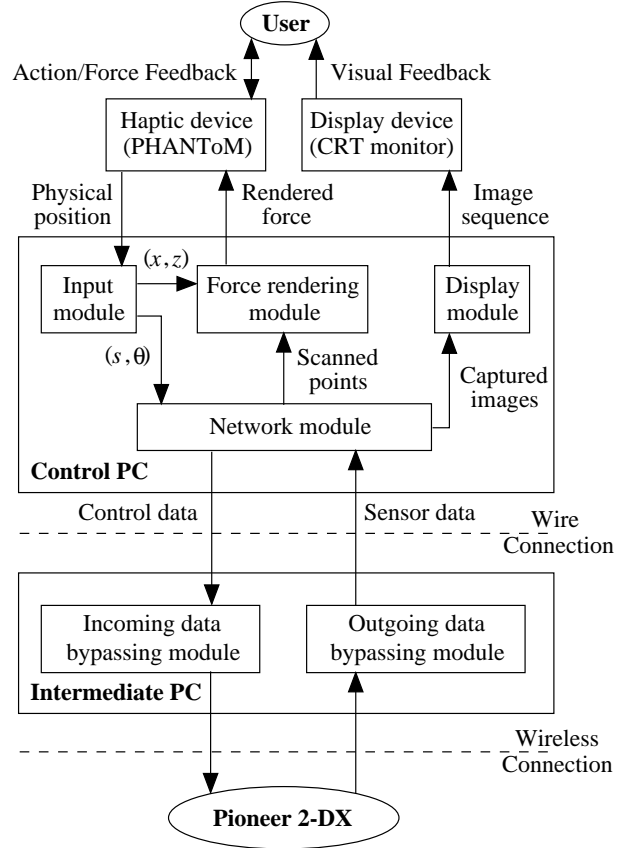


Figure 7: The system architecture.

resolution of 1 degree, a coverage of 180 degrees, and a distance range of approximately 8m at a scan rate of approximately 10Hz. We use the SensAble PHANToM as the force-feedback device.

The system architecture is shown in Figure 7. The system uses 2 PCs and an embedded PC in the Pioneer 2-DX. The control PC with PHANToM is indirectly connected to the Pioneer 2-DX via the intermediate PC since the control PC does not support a wireless network connection in our setup. The network connections of the control PC to the intermediate PC and the intermediate PC to Pioneer 2-DX have 100Mbps and 1Mbps bandwidths, respectively. The intermediate PC may be unnecessary if the control PC supports a wireless network connection.

In addition to force feedback, the system provides visual feedback of the image sequence captured by the camera attached to Pioneer 2-DX. The image update rate on the control PC is about 8Hz when the resolution of an image is 160×48 and each pixel is represented by 256 gray levels.

The input module converts a physical position of PHANToM to a logical position (x, z) , and maps the

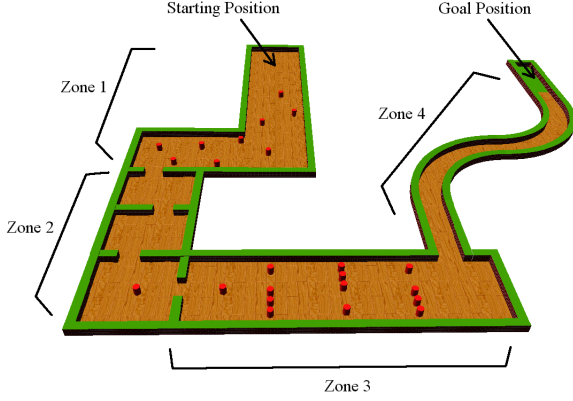


Figure 8: A perspective view of the virtual environment used for the experiment.

logical position to the motion parameters (speed rate s , turning rate θ) of the mobile robot by applying the car-driving metaphor described earlier. Although the PHANToM provides 3DOF position information, we ignore one DOF. In our implementation, a logical position is same as a physical position in the unit of mm but the y value is not used. The system uses $r = 30.0$, $k_1 = 20.0$ and $k_2 = 1.0$ in Equations (1) and (2) for the car-driving metaphor, and limits the working area of PHANToM to $200mm \times 200mm$, so that the speed rate and the turning rate of the robot are at most $1.4 m/sec$ and $70 degrees/sec$ respectively.

6 Experiment

We performed experiments to measure the effectiveness of haptic information to operators in safely navigating a robot in a given environment. In the experiments, three different methods for force rendering (independent variable) were compared with each other. The three methods can be distinguished according to the values of the constants k_3 , k_4 , k_5 and k_6 as follows:

- NF: No force feedback ($k_3 = 0$, $k_4 = 0$, $k_5 = 0$ and $k_6 = 0$).
- EF: Using the environmental force only ($k_3 = 0.1$, $k_4 = 0.1$, $k_5 = 0$ and $k_6 = 0$).
- EF & CF: Using both the environmental and the collision-preventing force ($k_3 = 0.1$, $k_4 = 0.1$, $k_5 = 0.3$ and $k_6 = 0.3$).

6.1 Virtual Environments

For experimental convenience, a virtual environment was used. In the experiment, a subject was required to make the robot navigate a virtual environment of size $13.8m \times 13.5m$. A perspective view of the

virtual environment used for the experiment is shown in Figure 8.

The virtual environment had two types of obstacles. One was the wall type (obstacles of width $0.2m$), and the other was the cylinder type (obstacles of diameter $0.15m$). All obstacles had the height of $0.2m$.

The obstacles were arranged in four different ways: scattering cylinders, the blocked walls, the cylindrical walls and the curved wall. In the zone of scattering cylinders (zone 1 in Figure 8), the distances between cylinders were between $0.7m$ and $1.5m$. In the zones of the blocked walls and the cylindrical walls (zone 2 and zone 3 in Figure 8 respectively), the widths of the openings in the walls were $0.5m$ and the distances between the walls were $1.4m$. In the zones of the curved wall (zone 4 in Figure 8), the widths of the road were $0.6m$.

In the virtual environment, the robot was shaped like a box that had the width of $0.35m$, the depth of $0.55m$ and the height of $0.25m$. When $\mathbf{P}(t) = [P_x(t) P_z(t)]^T$, $\mathbf{D}(t) = [D_x(t) D_z(t)]^T$, $s(t)$ and $\theta(t)$ represent the position, the direction, the speed rate and the turning rate of the robot at time t respectively, the motion of the robot is modeled as follows:

$$\begin{aligned} \mathbf{P}(t) &= \mathbf{P}(t - \Delta t) + s(t - \Delta t)\mathbf{D}(t - \Delta t)\Delta t \\ \mathbf{D}(t) &= \mathbf{R}(\theta(t - \Delta t)\Delta t)\mathbf{D}(t - \Delta t) \end{aligned}$$

where

$\mathbf{P}(0)$: initial position

$\mathbf{D}(0)$: initial direction

$$\mathbf{R}(\theta) = \begin{pmatrix} \cos \theta & \sin \theta \\ -\sin \theta & \cos \theta \end{pmatrix} : \text{rotation matrix}$$

Δt denotes the time interval between the previous frame and the current frame. Note that $s(t)$ and $\theta(t)$ are given from the logical position of the interface at time t .

The simulated robot had two virtual laser scanners to cover 360 degrees and a virtual camera on its top-center. The virtual laser scanner was simulated with the same specification as the real one described earlier. The virtual camera had a field of view of 45 degrees and the aspect ratio of 1.33:1.

In addition to the scene shown through the virtual camera, the virtual environment provides visual feedback in order to let subjects know when the robot collides with the obstacles, by changing the background color from blue to red. The background color returns to blue after 0.5 seconds.

6.2 Experimental Design

A subject was required to make the robot navigate the virtual environment from the start position to

the goal position as fast and carefully as possible. Although we assume that there is not a goal position in the actual use of the system, we overlaid a start position and a goal position in the virtual environment in order to collect experimental data.

A repeated measure design was applied to the experiment. A subject made one trial of the task with each force rendering method in a round (three trials total in a round) and repeated three rounds of trials, so that each subject made a total of nine trials of the task (three trials for each method). There was no break time between the trials. The methods were ordered differently for each subject, and subjects were not notified which method they were using.

Each subject had a training session before the experimental session not only in order to learn the usage of the interface but also in order to understand the task. In the training session, a subject made one trial of the task with each method. The virtual environment used for training was similar to that used for the experiment but the former had a smaller number of obstacles than the latter and did not have curved walls.

Twenty subjects voluntarily participated in the experiment. The ages of the subjects were between 20 and 35, and all of the subjects except two were male.

7 Experimental Results

In our experiments we measured the following seven dependent variables.

- The number of collisions
- Navigation time
- Average speed
- The minimum distance between the robot and the obstacles (over all directions, front direction (d_{front}) only, and rear direction (d_{rear}) only)
- The possible-turning angle (left angle (δ_{ccw}), and right angle (δ_{cw}))
- Speed on colliding with the obstacles (average and maximum)
- Turn rate on colliding with the obstacles (average and maximum)

Due to the lack of space, we present results only for three dependent variables i.e. the number of collisions, the navigation time and the minimum distance between the robot and obstacles. These are summarized in Figure 9 and Table 1.

The ANOVA and Tukey HSD post-hoc analysis on the results for the 3rd round revealed significant statistical differences among the methods on the number of collisions and the minimum distance ($p < 0.01$

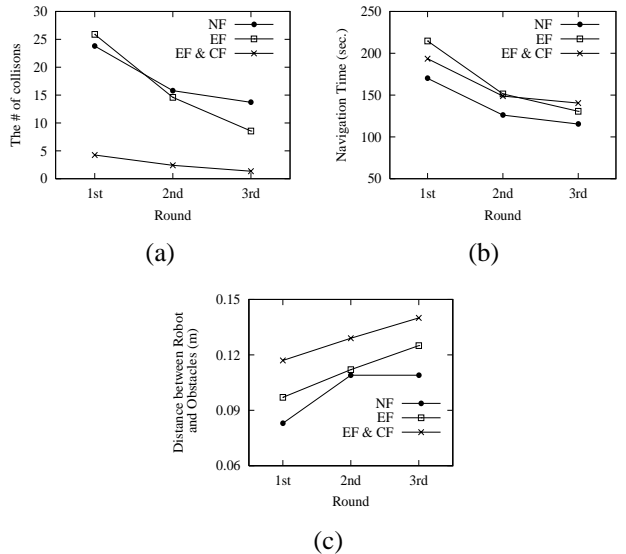


Figure 9: Experimental results: (a) number of collisions, (b) navigation time, and (c) minimum distance between the robot and obstacles.

for the number of collisions and $p < 0.05$ for the minimum distance). However, there were no significant statistical differences among the methods on the navigation time. This means that haptic information significantly improved some aspects of user performance (reduced number of collisions and larger distance of minimum approach to obstacles) without any degeneration in others (the navigation time). Although the number of collisions was dramatically reduced, it was not zero. In the experiment, the collision-preventing force did not completely prevent collisions. This is because the PHANToM generates forces that are too small to prevent users' actions. Nevertheless, 7 subjects were able to navigate the robot without any collisions.

8 Conclusion

We have measured the effectiveness of force feedback in a mobile robot teleoperation system for safe navigation in a shared autonomy scenario. Our system helps in the resolution of conflicts between operator intentions and the goals of the on-board controller. Our experiments (conducted using a virtual environment) measure the extent to which haptic information helps an operator in safely navigating a mobile robot. User studies indicate that the improvement in operator performance along several dimensions (the number of collisions, the minimum distance between the robot and the obstacles) due to haptic feedback is significant. This is accomplished without degradation in other aspects of performance such as navigation time.

Table 1: *Experimental results (mean and standard deviation) and the within-subject ANOVA results for the 3rd round.*

(a) The number of collisions: $F_{2,38} = 31.39$, $p < 0.0001$

	1st Round	2nd Round	3rd Round
NF	23.8(11.4)	15.8(11.7)	13.7(8.99)
EF	25.9(22.5)	14.6(14.1)	8.55(4.68)
EF&CF	4.25(5.09)	2.4(2.66)	1.35(1.57)

(b) The navigation time (sec.): $F_{2,38} = 3.04$, $p > 0.05$

	1st Round	2nd Round	3rd Round
NF	170.0(111.5)	126.1(89.5)	115.4(72.2)
EF	214.7(170.3)	151.4(98.3)	130.6(83.9)
EF&CF	193.5(92.3)	148.8(73.7)	140.5(84.9)

(c) The minimum distance (m): $F_{2,38} = 14.02$,
 $p < 0.0001$

	1st Round	2nd Round	3rd Round
NF	0.083(0.026)	0.109(0.028)	0.109(0.032)
EF	0.097(0.021)	0.112(0.029)	0.125(0.031)
EF&CF	0.117(0.024)	0.129(0.023)	0.140(0.020)

Acknowledgments

The authors would like to thank the Ministry of Education of Korea for its financial support toward the Electrical and Computer Engineering Division at POSTECH through its BK21 program. This work was supported in part under the Integrated Media Systems Center, a National Science Foundation Engineering Research Center at the University of Southern California.

References

- [1] T. Sheridan. *Telerobotics, Automation, and Human Supervisory Control*. MIT Press, Cambridge, MA, 1992.
- [2] R. Murphy and E. Rogers. Cooperative assistance for remote robot supervision. *Presence*, 5(2):224–240, 1996.
- [3] T. Fong, F. Conti, S. Grange, and C. Baur. Novel interfaces for remote driving: gesture, haptic and pda. In *SPIE Telemanipulator and Telepresence VII*, Boston, MA, USA, November 2000.
- [4] A. Bejczy and J. Salisbury. Kinematic coupling between operator and remote manipulator. *Advances in Computer Technology*, 1:197–211, 1980.
- [5] B. Hannaford, L. Wood, D.A. McAfee, and H. Zak. Performance evaluation of a six-axis generalized force reflecting teleoperator. *IEEE Transactions on Systems, Man, and Cybernetics*, 21(3):620–633, 1991.
- [6] T. H. Massie and J. K. Salisbury. The phantom haptic interface: A device for probing virtual objects. In *the ASME Winter Annual Meeting, Symposium on Haptic Interfaces for Virtual Environment and Teleoperator Systems*, Chicago, IL, USA, November 1994.
- [7] Immersion. Cybergrasp: Groundbreaking haptic interface for the entire hand. <http://www.immersion.com/products/3d/interaction/cybergrasp.shtml>.
- [8] Immersion. Gaming joysticks, wheels & gamepads. <http://www.immersion.com/products/ce/gamingjoystick.shtml>.
- [9] T. G. Anderson. A virtual universe utilizing haptic display. In *the First PHANToM User's Group Workshop*, Dedham, MA, USA, September 1996.
- [10] W. Aviles and J. Ranta. A brief presentation on the vrdfs - virtual reality dental training system. In *the Fourth PHANToM User's Group Workshop*, Deham, MA, USA, October 1999.
- [11] I. Elhaji, N. Xi, and Y. H. Liu. Real-time control of internet based teleoperation with force reflection. In *IEEE ICRA 2000*, San Francisco, CA, USA, April 2000.
- [12] M. L. McLaughlin, G. Sukhatme, C. Shahabi, J. Hespanha, A. Ortega, and G. Medioni. The haptic museum. In *the EVA 2000 Conference on Electronic Imaging and the Visual Arts*, Florence, Italy, 2000.
- [13] M. A. Srinivasan and C. Basdogan. Haptics in virtual environments: Taxonomy, research status, and challenges. *Computers & Graphics*, 21(4):393–404, 1997.
- [14] D. Xiao and R. Hubbard. Navigation guided by artificial force fields. In *ACM CHI 98 Conference on Human Factors in Computing Systems*, Los Angeles, CA, USA, April 1998.
- [15] D. Bartz and Ö. Güvit. Haptic navigation in volumetric datasets. In *PHANToM User Research Symposium*, Zürich, Swiss, 2000.
- [16] I. Elhaji, N. Xi, W. K. Fung, Y. H. Liu, W. J. Li, T. Kaga, and T. Fukuda. Haptic information in internet-based teleoperation. *IEEE/ASME Trans. on Mechatronics*, 6(3):295–304, September 2001.
- [17] T. Fong, C. Thorpe, and C. Bauer. Advanced interfaces for vehicle teleoperation; collaborative control, sensor fusion displays, and remote driving tools. *Autonomous Robots*, 11:77–85, 2001.
- [18] O. Khatib. Real-time obstacle avoidance for manipulators and mobile robots. *The International Journal of Robotics Research*, 5(1), 1986.